NANOMEDICINE

A flexible drug delivery chip for the magnetically-controlled release of anti-epileptic drugs ☆

Wei-Chen Huang, Shang-Hsiu Hu, Kun-Ho Liu, San-Yuan Chen *, Dean-Mo Liu *

Department of Materials Sciences and Engineering, National Chiao Tung University, Hsinchu, 30010, Taiwan

ABSTRACT

A flexible drug delivery device was designed and fabricated using electrophoretic deposition of drug-carrying magnetic core-shell Fe_3O_4 at SiO_2 nanoparticles onto an electrically conductive flexible PET substrate. The PET substrate was first patterned to a desired layout and subjected to deposition. In doing so, a uniform and nanoporous membrane could be produced. After lamination of the patterned membranes, a final chip-like device of thickness less than 0.5 mm is formed that is used for controlled delivery of an anti-epileptic drug, i.e., ethosuximide (ESM). The release of useful drugs can be controlled by directly modulating the magnetic field, and the chip is capable of demonstrating a variety of release profiles (i.e., slow release, sustained release, step-wise release and burst release profiles). These profiles can follow a wide spectrum of patterns ranging from zero to pulsatile release kinetics depending on the mode of magnetic operation. When the magnetic field was removed, the release behavior was instantly ceased, and vice versa. A preliminary in-vivo study using Long–Evans rat model has demonstrated a significant reduction in spike-wave discharge after the ESM was burst released from the chip under the same magnetic induction as in-vitro, indicating the potential application of the drug delivery chip. The flexible and membrane-like drug delivery chip utilizes drug-carrying magnetic nanoparticles as the building blocks that ensure a rapid and precise response to magnetic stimulus. Moreover, the flexible chip may offer advantages over conventional drug delivery devices by improvement of dosing precision, ease of operation, wider versatility of elution pattern, and better compliance.

© 2009 Elsevier B.V. All rights reserved.

1. Introduction

The design of a novel drug delivery system for specific disease treatment has been a technically and pharmaceutically important objective that has received increased attention worldwide. The most frequently considered dosing mechanisms include oral administration, injection-type administration, or implantable systems for controllable drug release [1–3]. Among these, implantable drug delivery systems near the site of disease have been considered clinically valuable because of their ability to provide rapid or constant dosing over a longer period of time. This medication approach is particularly applicable to chronic disorders such as neurological disorders, alcohol poisoning, etc. Treatment of epileptic disorders is especially relevant, as these neurological disorders threaten approximately 4% of the global population [4].

The treatment of this neurological disorder signifies an important role in the field of modern medicine. Today, 70% of patients can be treated using systemic methods, although taking advantage of systemic methods usually requires the penetration of the drug through the blood–brain barrier (BBB) [4,5]. This approach results in much of the drug remaining outside of the BBB. Thus, only a small amount of the drug actually serves its medicinal purpose, which reduces therapeutic efficacy considerably. For this reason, an implantable drug delivery device that can be inserted into the temporal lobe of one's brain is potentially promising, as it would allow for the release of an anticonvulsant drug at a constant rate without resistance from the BBB [6–8].

Currently, implantable drug delivery systems have had rigid structural designs, such as silicon-based drug delivery chips [9] and ceramic-based skeletal drug delivery packages [10], which can require extensive invasive surgery or reduce the patient's post-implantation compliance. After implantation, drug delivery in these systems may proceed in an un-controlled manner, such as free diffusion, or with merely a pre-programmed profile. Unfortunately, such designs may impart a high risk to the patients if the physiological conditions of the patient change unexpectedly. In such circumstances, a corresponding change in the dosing amount would be desirable, and in certain conditions, it may be necessary to stop dosing entirely. To prepare for a variety of physiological and psychological complications, it is necessary to design a novel drug delivery device that is flexible in structure, small in size, and capable of providing remotely triggered (i.e., induction by magnetic fields) drug release with a desirable profile. Aside from these technical issues, it is even more clinically

important for the drug delivery device to regulate the release of the drug in a controllable and switchable profile, such as between a sustained and pulsatile pattern, with precise dosage control, to adequately control a variety of potential clinical complications.

In our previous study, we designed core-shell magnetic field-sensitive nanoparticles capable of delivering active agents in a controllable manner by tuning an applied magnetic field [11–13]. By taking advantage of electrophoretic deposition (EPD) methods [14–20], we attempt to use such nanoparticles as building blocks to form a nanoporous membrane that can be driven under a given electric field to aggregate onto a flexible, electrically conductive electrode. These core-shell nanoparticles are composed of magnetic nanoparticulate Fe_3O_4 multi-cores deposited with a thin shell layer of SiO_2 (symbolized as Fe_3O_4 at SiO_2). Ethosuximide, chemically designated as alpha-ethyl-alpha-methyl-succinimide, is a water-soluble drug and a proposed T-type Ca^{2+} channel blocker. It has been successfully employed to eliminate partial seizures and has long been used as the first-choice therapeutic agent to ameliorate clinical spike-wave discharge (SWD) occurrences. As such, ethosuximide is used in this investigation as the model drug to demonstrate controlled release. However, due to the use of a rat model, size limitation restricts chip implantation into rat's brain; instead, peritoneum of the rats was selected for this investigation, to evaluate the feasibility of this new type of drug delivery chip in anti-epileptic treatment in-vivo.

2. Experimental procedures

2.1. Synthesis of core-shell Fe_3O_4 at SiO_2 nanoparticles

Core-shell Fe_3O_4 at SiO_2 nanoparticles were synthesized via conventional microemulsion and sol–gel technology as previously described [21,22]. In short, the first step is to synthesize the monodispersed superparamagnetic iron oxide nanoparticles (Fe_3O_4) via a high-temperature decomposition of $Fe(acac)_3$. Two key steps were employed to form these monodispersed nanoparticles: first, the growth of nuclei was carried out at 200 °C, then the reaction temperature was raised to 300 °C, permitting the iron oxide nanoparticles to grow to uniform size. The iron oxide nanoparticles show an average diameter of 5 nm. To design the core-shell structure, a small amount, 0.5 ml, of the Fe_3O_4 suspension was added to 7.7 ml cyclohexane to create the oil phase, while the water phase was composed of 1.6 ml hexanol and 0.34 ml H_2O. Next, these two phases were mixed following the addition of 2 g octyl phenol ethoxylate as the surfactant to form a water-in-oil phase. After adding 2 g of TEOS and aging for 6 h, the water-in-oil solution was utilized in a sol–gel process with 1 ml NH_4OH. This permitted hydrolysis and condensation reactions to occur, thereby allowing the nanoparticle to be formed through gelation. The synthesized nanoparticles were then examined under a transmission electron microscope (TEM, JEM-2100, Japan) and characterized using electrophoretic light scattering (ELS) for zeta potential determination.

2.2. Drug encapsulation

In order to incorporate the hydrophilic anticonvulsant drug, ethosuximide (ESM), into the core-shell nanoparticles, the drug was first dissolved completely in aqueous solution, with a concentration of 5 wt.%. The drug was incorporated using the emulsification process described previously for the synthesis of Fe_3O_4 at SiO_2 nanoparticles. After drug encapsulation within the core phase of the nanoparticle, a subsequent SiO_2 layer deposition was applied to form a thin outer shell phase, acting as a barrier to regulate the drug release profile. The final drug-containing nanoparticle suspension was found to be relatively stable for at least 24 h in ethanol, as no sign of sedimentation was detected during that time period.

2.3. Electrophoretic deposition of ESM nanocarriers

To set up an EPD cell, an ITO (In-doped SnO_2)-coated conducting flexible plate (PET substrate, JoinWill Tech.Co., Ltd., Taiwan, having an electrical resistance of 50 Ω/sq) with dimensions of 20 mm × 50 mm × 0.02 mm was used as an anode and was patterned by lamination with PVC tape for three side walls of the substrate in advance (Fig. 1), leaving one side unsealed as the outlet for drug elution. Final lamination of the substrate was performed at a later stage of the assembly. The area of the PET substrate that can be used for membrane deposition is pre-designed to be 1 cm² (1 cm × 1 cm). A stainless steel plate (316 L) with dimensions of 20 mm × 50 mm × 0.02 mm (YEONG-SHIN Co., Ltd., Taiwan) was used as cathode and was carefully cleansed sequentially by sonication in acetone, ethanol, and deionized water at room temperature. After the cathode was cleaned and rinsed, it was then dried by blowing with nitrogen gas. A pair of parallel electrodes with 2 cm separation was set vertically in a glass beaker containing the colloidal suspension with 5 wt.% of the ESM-containing nanoparticles under magnetic agitation. A constant dc voltage (30 V) was applied between two electrodes for 10 min. After deposition, the substrate was carefully withdrawn from the glass beaker and dried at room temperature for 1 h. After the first deposition (as the first layer), the flexible substrate was subjected to further coating with a thin layer of sputtered gold to cover the membrane. The purpose of the thin gold coating is twofold; first, it prevents undesired detachment of the deposited nanoparticles from the first layer, and second, it imparts conductivity for further deposition. Following the same procedure, the second and third layers of the coatings were carried out to form the final drug-carrying component.

2.4. In-vitro drug release study

A sandwich structure of the drug delivery chip can be produced by laminating two sets of the drug-carrying components in a "(PET–
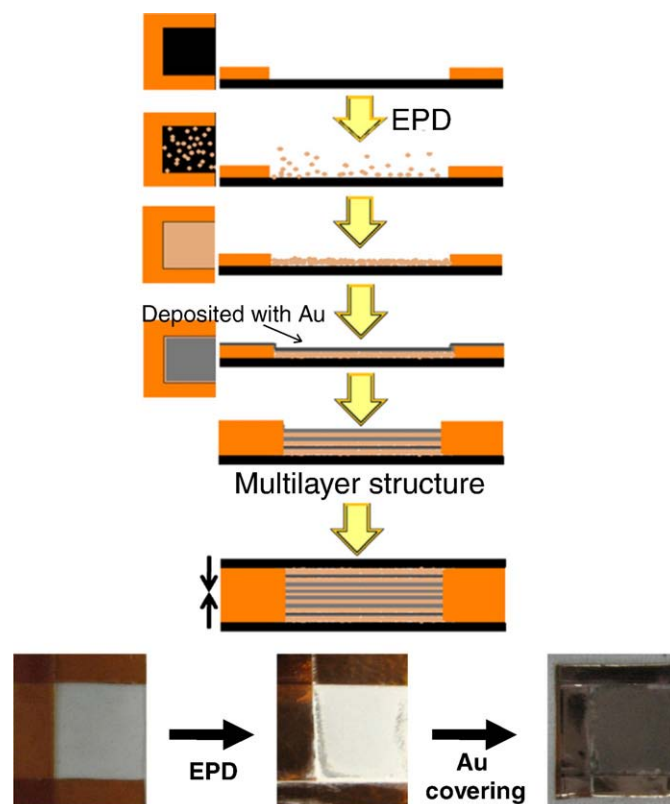

Fig. 1. Schematic flowchart of the preparation details of the multilayer membrane and construction of the drug delivery chip.

membrane)–(membrane–PET)" configuration. This resulted in one side of the chip remaining exposed to the surrounding environment thereby providing an outlet for drug elution. The experimental setup is presented schematically in Fig. 2A. The resulting chip-like device, which has a total thickness of less than 0.5 mm and demonstrates mechanical flexibility, was then immersed in a phosphate buffer solution (at pH 7.4) to test its capabilities in drug release (Fig. 2B). A magnetic field was generated, using a home-made AC magnetic generator, with a constant frequency of 70 kHz to trigger drug elution from the flexible drug-carrying chip to examine the release capabilities of said chip. Drug concentration before and after the release tests was assessed using reverse phase high-performance liquid chromatography (HPLC, AGILENT TECHNOLOGIES Co., Ltd., Taiwan). Drug solutions were handled at a constant volume of 50 μL which was injected into the HPLC. The Diode Array Detector was set at 217 nm to detect the anti-epileptic drug, ESM. The mobile phase consisted of 50% water, as phase A, and 50% methanol, as phase B, with a flow rate of 1.0 ml/min, a gradient elution profile of 5.0–50.0% B with a linear ramp from 0–5 min, 50.0–5.0% B with a linear ramp from 5–10 min, and finally, a 10-minute washout period. Drug-free Fe_3O_4 at SiO_2 suspensions were prepared as standard controls by immersing Fe_3O_4 at SiO_2 particles in water at a concentration of 3% v/v. Test samples were prepared using the same procedure, where 3% v/v Fe_3O_4 at SiO_2 encapsulated with ESM was used for drug release tests under various durations of magnetic induction. A two-parameter quadratic equation, with an intercept at the origin, was used to produce a calibration curve for the ethosuximide by integrating the standard peak area ratio. The metabolite was assumed to have the same peak area response per mole as ethosuximide; hence, the ethosuximide calibration curve was used to quantify the metabolite level [23].

2.5. In-vivo study

Adult male Long–Evans ($N = 60$) were randomly divided into 4 treated groups ($n = 15$ in each group) and Wistar rats were used as described above. All rats were kept in a sound-attenuated room under a 12:12 h light–dark cycle (07:00–19:00 lights on) with food and water provided ad libitum. The experimental procedures were reviewed and approved by the Institutional Animal Care and Use Committee. Briefly, the recording electrodes were implanted under pentobarbital anesthesia (60 mg/kg, i.p.). Subsequently, the rat was placed in a standard stereotaxic apparatus. In total, six stainless steel screws were driven bilaterally into the skull overlying the frontal (A +2.0, L 2.0 with reference to the bregma) and occipital (A −6.0, L 2.0) regions of the cortex to record cortical field potentials. A ground electrode was implanted 2 mm caudal to lambda. Dental cement was applied to fasten the connection socket to the surface of the skull. Following suturing to complete the surgery, animals were given an antibiotic (chlortetracycline) and housed individually in cages for recovery.

Long–Evans rats are used because they often display spontaneous SWDs, which have been demonstrated to be associated with the absence of seizures in several aspects of evidence. In this preliminary animal test, we compared the effect among saline, ethosuximide (ESM), ESM-containing nanoparticles (ESM-Fe_3O_4 at SiO_2) and ESM with the chip (ESM-Chip) in spontaneous SWDs of Long–Evans rats. The chip with dimensions of 5 mm × 5 mm × 0.02 mm was prepared and implanted into the peritoneum of the rats, while the other three doses were subjecting to IP injection.

3. Results and discussion

3.1. Core-shell nanoparticle synthesis

The core-shell Fe_3O_4 at SiO_2 nanoparticles, as described previously [22], showed a spherical geometry having a mean particle diameter of about 300 nm. Nanometric magnetic particles were embedded and distributed randomly within the core, followed by deposition of a thin silica shell. As demonstrated in a previous study, these magnetic nanoparticles exhibit an Fe_3O_4 crystallographic ferrite structure [24]. The silica shell has a thickness of about 5–10 nm. Transmission electron microscopy images, seen in Fig. 3, show that the silica shell exhibits a relatively compact structure, where no appreciable pores are detectable under high microscopic resolution. This suggests that such a silica shell is able to act as a regulator that controls the passage of drug molecules from the core phase. In particular, no appreciable elution of the drug from the core-shell particle was observed in the absence of a magnetic stimulus, which will be discussed in forthcoming analyses.

3.2. Drug release profile from Fe_3O_4 at SiO_2 nanoparticles

The Fe_3O_4 at SiO_2 nanoparticles associated with the encapsulated anticonvulsant drug, ethosuximide (ESM), have been successfully prepared by in-situ microemulsion followed by a sol–gel consolidation method. The ESM encapsulated within the Fe_3O_4 at SiO_2 nanoparticle was confirmed using FTIR analysis, as shown in Fig. 4 where
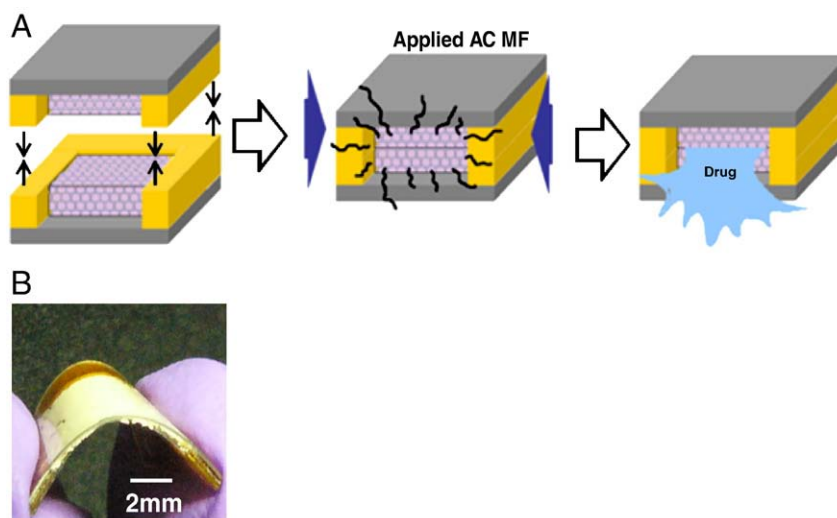

Fig. 2. (A) Schematic of the sandwich structure of a magnetic field-sensitive drug delivery chip designed in this study. (B) The resulting chip-like device exhibits mechanically flexible characteristics.
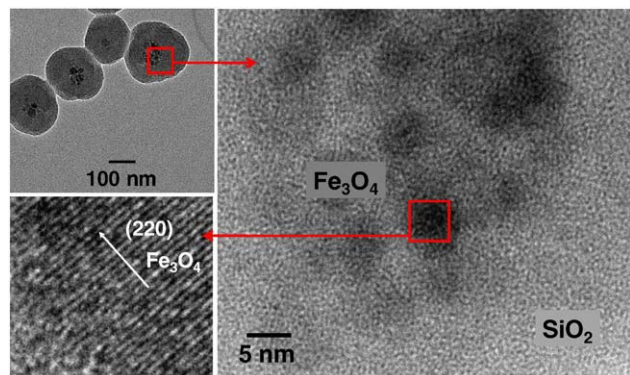
Fig. 3. High resolution transmission electron microscopy images of Fe_3O_4 at SiO_2 nanoparticles where a detailed nanostructure and phase distribution are clearly illustrated.
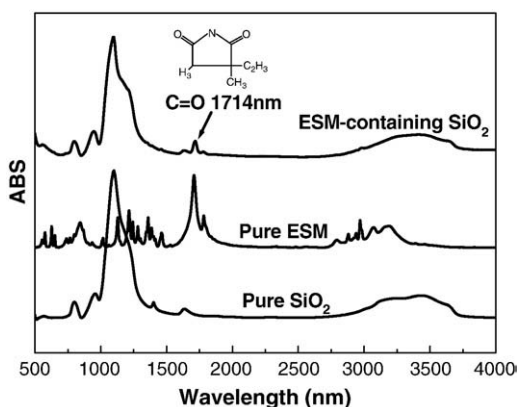
Table 1
Zeta potential analysis reveals the IEP of the nanoparticles located over a wide range of pH from ~3 to ~12.

pH value	Zeta potential of SiO_2 (mV)	Zeta potential of SiO_2 at Fe_3O_4 (mV)
2.85	− 36	− 11
5.48	− 51.6	− 41.3
9.06	− 53.5	− 42.9
11.82	− 54.2	− 47

the field, aliquot amounts of the buffer solutions were withdrawn at 10-second intervals, the concentration of ESM released was measured via HPLC, and the cumulative amount of drug release was determined using Eq. (1):

$$Cumulative\,released\,(\%) = \frac{R_t}{L} \times 100\% \qquad (1)$$

where L and R_t represent the initial amount of drug loaded and the cumulative amount of drug released at time t, respectively.

There is little or no release detectable in the absence of the magnetic field. Although a small amount of drug (about 4–5%), which reaches a relatively constant level after only 20 s of immersion, was measured. It is believed that this represents the washing off of surface residue remaining from nanoparticle preparation. Nonetheless, the vast majority of ESM is released (~100%) with a relatively short induction period (30–40 s). This indicates a burst release profile that can be easily managed. This test not only reveals an encapsulation efficiency of about 10%, but the resulting release profiles also suggest the fast-response behavior of the SiO_2 at Fe_3O_4 nanoparticles to magnetic induction.

3.3. Characterization of the Fe_3O_4 at SiO_2 membrane

Zeta potential analysis reveals that the IEP of the nanoparticles is located in a highly-acidic region, as given in Table 1. As such, the Fe_3O_4 at SiO_2 nanoparticles show an increasingly negative charge over a wide pH range of ~3 to ~12. In comparison to the zeta potential of pure SiO_2 nanoparticles, it appears that the incorporation of Fe_3O_4 could slightly neutralize the negative charging of the silica shell. The highly negative charged Fe_3O_4 at SiO_2 nanoparticles, after re-dispersing in ethanol, showed a relatively stable suspension for at least 24 h.

Under a constant electrical field of 30 V, the drug-carrying nanoparticles deposited onto the anodic substrate and reached a thickness of ~22 μm with a deposition time of 10 min, corresponding to a deposition rate of about 2.2 μm/min. Scanning electron microscopy revealed that a uniform and porous coating can be formed (Fig. 6),

Fig. 4. Fourier Transform Infrared Spectroscopy spectra of Fe_3O_4 at SiO_2 nanoparticles, ESM, and ESM-carrying nanoparticles.

the characteristic peak at the position of 1714 nm^{-1} designates the C O bond in ESM for the ESM-containing nanoparticles. The amount of ESM associated with the nanoparticles was determined by applying a magnetic field to allow the complete release of the drug into the environment within a short magnetic induction period, as demonstrated in an earlier study [22].

Fig. 5 shows the drug release profiles for the Fe_3O_4 at SiO_2 nanoparticles with and without magnetic induction. The full strength of the magnetic field is 2.5 kA/m. Under the full magnetic strength of
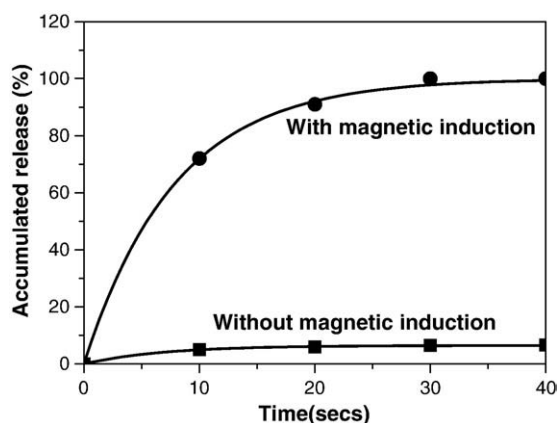

Fig. 5. Drug release profiles for the ESM-containing core-shell nanoparticles. In the presence of the magnetic field treatment, fast release kinetics are demonstrated, while a near-zero release was observed without the magnetic induction treatment.
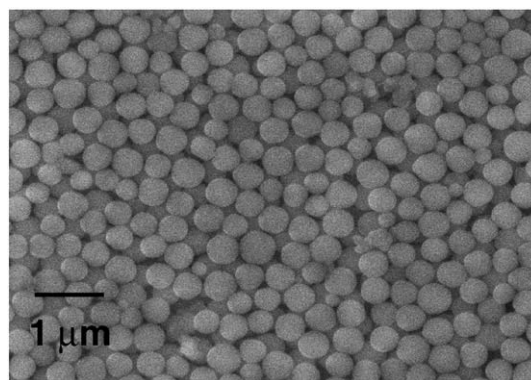

Fig. 6. The SEM image at higher magnification reveals a structurally uniform and nanoporous morphology of the coating on the substrate. This suggests that Fe_3O_4 at SiO_2 nanoparticles can be successfully assembled onto the flexible substrate, with an orderly packing configuration.

indicating that the Fe_3O_4 at SiO_2 nanoparticles can be successfully assembled with an orderly-arranged configuration, on the flexible substrate. The second and third layers of the nanoparticle-assembled membranes can be deposited consecutively after a thin coating of Au is applied.

After ambient drying, a structural analysis showed that the resulting multilayer membrane exhibits a thickness of about 70 μm and demonstrates excellent structural integrity. Additionally, no considerable delaminated fragments were ever detected. Microscopic examination also indicated a well-packed configuration of the drug nanocarriers, leaving nanometric inter-particle voids distributed uniformly throughout the entire membrane. Such a well-packed nanostructure is suggested to stem from strong inter-particle repulsion occurring as a result of the nanoparticles substantial negative charge. The zeta potential reaches a level of about −42 mV at neutral conditions, which should energetically regulate the assembly of the nanoparticles upon impact with the anodic substrate. Despite this, estimates indicate that about 350 nanoparticles reach the substrate over a surface area of 1 μm²/min.

The interconnected nanoporous network, developed as a result of the nanoparticle packing, is beneficial for allowing a fluid flux of drug out into the surrounding environment. Additionally, the network may also provide reservoirs that permit refilling of the drug into the device for subsequent medication purposes, if such a process is deemed practical.

3.4. Magnetic-driven drug release behavior

Fig. 7A shows the release profiles of ESM from the flexible chip under magnetic fields (MF) of varying strengths: 0 A/m (i.e., no MF),

Fig. 7. (A) ESM release profiles of the flexible chip under continuous stimulation of different magnetic field strengths. (B) A plot of $\ln(M_t/M)$ versus $\ln(t)$ of data from (A).

1.0 kA/m, and 2.5 kA/m. The amount of ESM released without magnetic induction was relatively low; about 9–10% over a time span of 60 min. In comparison, under a stronger magnetic field, 1.0 kA/m, 40% of ESM was released, and the strongest magnetic field, 2.5 kA/m, produced 100% drug release within the same 60-minute time period. These field-strength specific release profiles strongly indicate that the applied magnetic field effectively drives the release of the drug from the deposited membrane. A closer look at the release profiles in relation to induction shows the release is much faster in the first 15 min and is followed by a relatively slow and sustained release profile for the remaining time period. Such two-stage release behavior is totally different from that observed in the nanoparticulate form (Fig. 5), suggesting that this effect is characteristic of the chip design. The first-stage release is relatively fast and is due to a rapid response of the drug carriers to the induction. This is especially true for those drug nanocarriers near the outlet region of the chip. For the nanocarriers located in the inner region of the chip, a longer path length of diffusion is required, thereby increasing the tortuosity. This gives the apparent release profile a flatter kinetic pattern, even when the chip is subjected to constant magnetic induction. This observation also indicates that the resulting release profile can be easily manipulated through the structural design of the chip. Through experimental observation, we see this is the case, as chips with smaller dimensions have release profiles that are kinetically similar to those of individual nanocarriers. Chips of larger dimension, such as 1 cm × 1 cm × ~0.3 cm in the current study, possess release kinetics quite different from the behavior of its building block.

The apparent release kinetics for the chip can then be determined using Eq. (2) and the drug released data from Fig. 7A:

$$\frac{M_t}{M_\infty} = kt^n \qquad (2)$$

The cumulative concentration of released drug at time t and at the end was incorporated to calculate the fractional uptake M_t/M_∞, where k is a characteristic constant, and n is a characteristic exponent related to the transport mechanism within the matrix. For Fickian kinetics, the rate of diffusion is rate limiting at $n = 0.5$. Values of n between 0.5 and 1 indicate the contribution of non-Fickian processes such as a structural limit. It is important to note that this equation is valid for the first 60% of the normalized drug uptake. By taking the logarithm on both sides of Eq. (2), Eq. (3) can then be used to calculate the diffusion parameters (n and k).

$$\ln\left(\frac{M_t}{M_\infty}\right) = n \ln t + \ln k \qquad (3)$$

Taking advantage of Eqs. (2) and (3), a kinetic analysis of ESM release from the flexible chip can be obtained, as shown in Fig. 7B. Here, we see that only the first 60% of drug released was used for calculation, regardless of the magnetic field strength, as this range corresponds to the first-stage release of the chip. A linear relationship with a relatively high correlation coefficient (greater than 0.99) can be obtained from the regression analysis. In this analysis, the exponent constant (n) and rate constant (k) were estimated for all ranges of magnetic field strength including the case of no field induction. With no magnetic field induction, the apparent release profile is solely related to structure. In this case, we show an exponent value of 0.41, beyond the regime of Fickian diffusion mode. This may be a result of a physical barrier, i.e., the nanocarrier itself, arising in the chip that effectively inhibits the diffusion of drug release from the surface of the nanocarriers.

Actually, due to a number of factors including a none-perfect sealing of the device or a natural diffusion from the outlet, the gradual release with a relatively small amount of the ESM drug from the chip over a certain time period indeed has been addressed. However, comparing
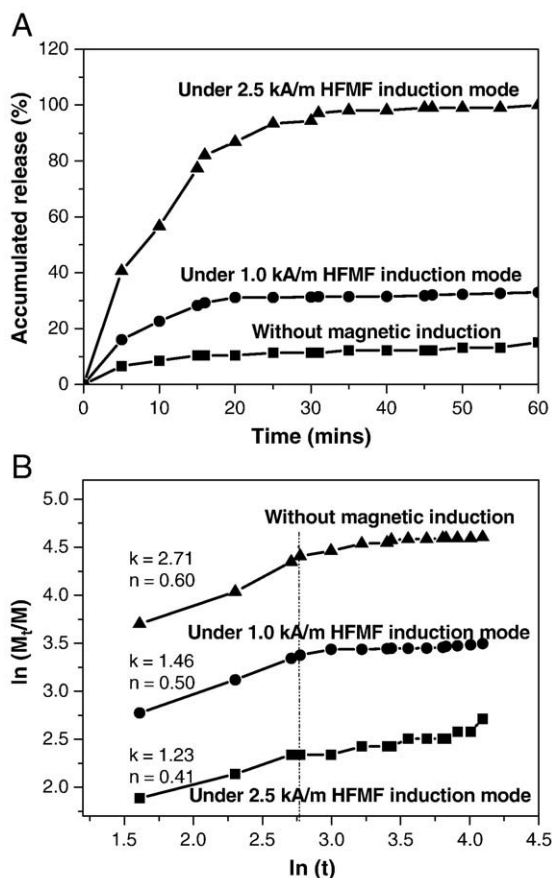
with drug elution as a result of magnetic stimulus, the gradual release becomes relatively minor (the in-vivo test showed a marked anti-epileptic efficacy only under magnetic exposure). A further work toward better mechanical sealing and structural modification of the device with optimal control of drug elution will surely be carried out in the near future, as an important engineering focus for practical uses.

For the other two release profiles under magnetic induction, the exponent constants (n) are all in a range of 0.5–0.6, indicating a typical Fickian diffusion mode. Accordingly, the Fickian-like diffusion pattern of ESM elution is virtually a combination of two paths. One path is from the nanocarrier itself (i.e., magnetic-induced expulsion of ESM from the core-shell nanoparticles towards the environment), having a relatively fast release kinetics, while the second is a free diffusion toward the outlet of the chip. For this reason, it is obvious that the second diffusion path provides evidence that the pure SiO_2 at Fe_3O_4 particles released drug faster than the processed chip under the same strength of magnetic induction, which can be confirmed by the data in Fig. 5. Moreover, the rate constant (k) in Fig. 7B increases with the strength of the magnetic field, suggesting a field-induced drug expulsion. This differs from the drug release mechanism outlined in a previous study [22] for individual nanocarrier. For this chip, one plausible explanation is due to the superparamagnetic heating of the Fe_3O_4 at SiO_2 nanoparticles under magnetic induction, where micro-metric or nano-metric scale fluid convection around the nanocarriers accelerates drug expulsion toward the environment. Therefore, a higher magnetic field strength, a larger dosing amount, and a higher rate of drug release can be finely controlled.

A step-wise change in the drug eluting profile can be detected at various time intervals upon repeated on–off magnetic operation, as is seen in Fig. 8. In the presence of magnetic induction, a rapid response in drug elution from the chip is observed with the form of a burst-like profile. With no induction, the drug eluting profile becomes relatively slow or even eliminated. From our understanding, the slower release profile is essentially a consecutive outward diffusion behavior of the drug from inside the chip. This is a direct result of rapid removal from the previous-stage induction, rather than a true release profile of the chip. On this basis, a zero- or near zero-release profile can be reasonably achieved, which provides another alternative drug release mode for the chip.

Such a burst-like release pattern can also occur via nanostructural perturbation of the core-shell nanoparticle. The rotation and move-ment of the embedded magnetic nanoparticles result in an expulsion of the drug molecules to the environment. Similar behavior can be applicable to the chip designed in this study. Moreover, even after considerable assembly of the nanoparticles into macroscopic agglom-erates, the burst-like release pattern still remains unchanged compared to the individual 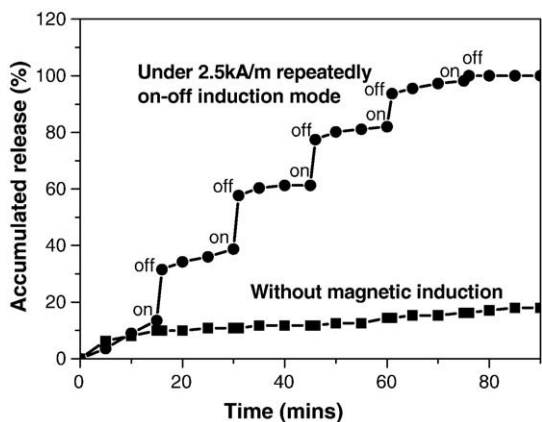pattern. This finding implies a benefit to employing low-dimensional carriers. Even in the case of a larger dimensional entity, a high-responsive behavior of individual carriers to the environmental stimuli ensures that a real-time response can be achieved in the larger assembly.

The burst-to-zero-to-burst release pattern can be repeated several times, which suggests that: (1) the nanostructural perturbation of the nanoparticles as a result of magnetic induction should be small enough to be considered an elastic behavior, (2) the mechanical fatigue of the building materials can be effectively reduced, even when it is assembled into larger dimensions, and (3) the chip is working well as a multiple-use drug delivery device capable of delivering drugs with a tunable release profile.

3.5. In-vivo study

In this preliminary in-vivo study, Fig. 9 depicts representative examples of spike-wave discharges (SWDs) after the administration of saline, ESM, ESM-Fe_3O_4 at SiO_2, and magnetically-induced ESM-Chip. The SWDs showed no obvious difference. In this experiment, we recorded 1-hour spontaneous brain activity before the treatment (baseline) and another 1-hour spontaneous brain activity 30 min after the treatment. The indexes were normalized by average of the two 1-hour baselines. In the conditions of administering ESM-Fe_3O_4 at SiO_2 and magnetically-triggered ESM-Chip, rats were restrained in a plastic box then put into the center of a coil following by magnetic stimulus (2.5 kA/m) as the one being aforementioned in-vitro to release ESM. Although it is hard to quantify the amount of the ESM released into the rats, it is surely indicated that the amount of ESM released, from both ESM-Fe_3O_4 at SiO_2 (Fig. 10B) and ESM-Chip (Fig. 10C), demon-strated significant effect in reducing the number and total duration of spontaneous SWDs, as comparing to ESM alone (Fig. 10A). Although a peritoneum implantation was employed, instead of brain site, con-trolled ESM release from these in-vivo data, albeit relatively pre-liminary, evidenced that the ESM with the nanoparticle and the chip can be successfully eluted through an external magnetic stimulus, as that observed in-vitro. In the meantime, the therapeutic efficacy of the ESM being eluted appeared to preserve its effect in SWD suppression [25].

4. Conclusions and implications

A novel flexible drug delivery chip-like device was successfully designed and fabricated using electrophoretic-based technology to bring a drug-carrying core-shell magnetic nanoparticle into a mem-brane. The chip was capable of delivering drugs with a fast and precise
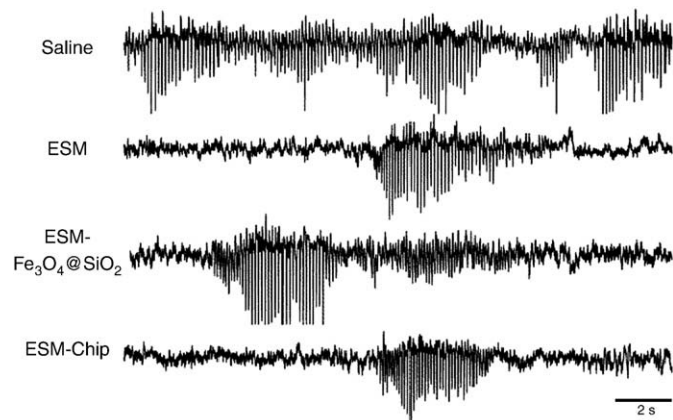

Fig. 8. Drug release behaviors of the chip under the various conditions of magnetic induction.

Fig. 9. Representative examples of spontaneous SWDs under intraperitoneal adminis-tration of saline, ethosuximide (ESM) (28 mg/kg, i.p.), ESM with the ESM-containing nanoparticles (ESM-Fe_3O_4 at SiO_2) (40 mg/kg, i.p.), and ESM with the chip (ESM-chip) (ca. 40 mg/kg, intraperitoneal implantation).
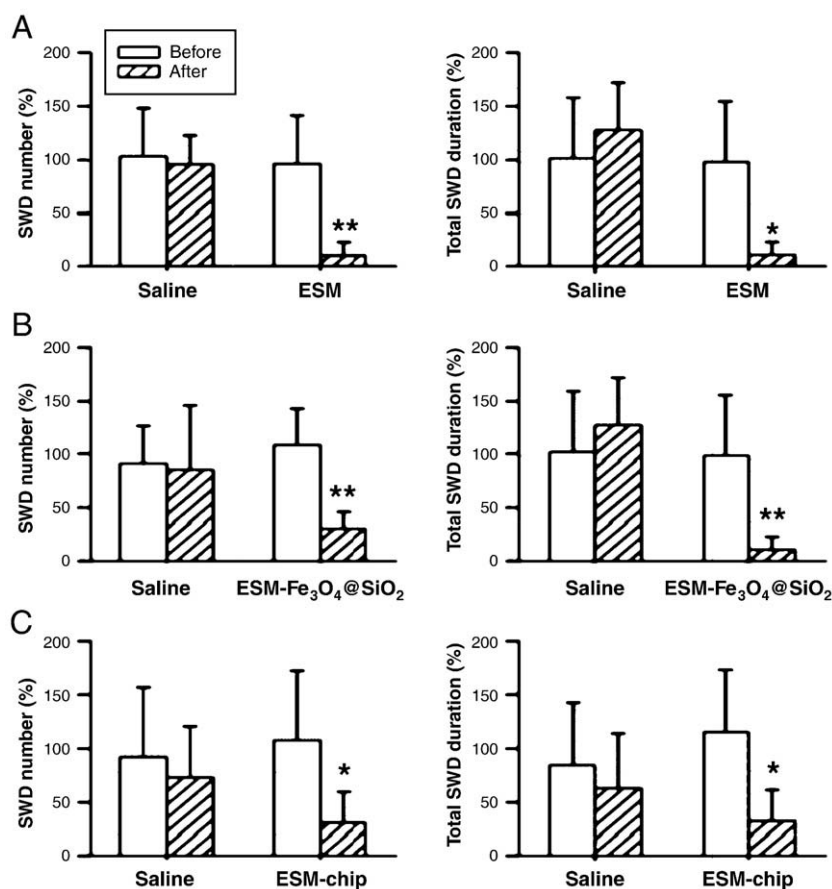
Fig. 10. Comparison of SWD number and total SWD duration with saline and 3 different forms of ESM in Long–Evans rats with spontaneous SWDs ($n = 8$). (A) ESM (0.5 ml, 28 mg/kg, i.p.) significantly decreased SWD number and total SWD duration. (B) ESM with the nanoparticles (ESM-Fe_3O_4 at SiO_2) (40 mg/kg, i.p.) significantly reduced SWD number and total SWD duration. (C) ESM with the chip (ESM-Chip) (ca. 40 mg/kg, intraperitoneal implantation) significantly reduced SWD number and total SWD duration. *$P < 0.01$; **$P < 0.001$.

response over a wide variety of release patterns, including sustained release, step-wise release, and burst release, according to the given operation mode of the magnetic field. It is expected that the rapid response of the drug-delivery chip may be used to pulse anti-epileptic drug into the surrounding environment under a given magnetic induction. This would suggest a potential use of the device for the prevention of seizures in patients suffering from epileptic disorders. However, it is more clinically desirable if the chip can be fabricated by better mechanical sealing and structural modification that the further integrated device with a signaling system can trigger the generation of a magnetic field for precise and timely drug delivery. Although at early stage of technical development, the drug delivery chip was further evaluated in an animal model. The preliminary data showed both the nanoparticles and the chip capable of eluting therapeutically effective amount of ESM by external magnetic stimulus to reduce significantly the SWD, thus, showing an effective anti-seizure behavior. As such, a more extensive and in-depth in-vivo study has been underdevelopment and the results are even more promising which will be reported separately. It is envisioned that such a flexible drug delivery chip can be used as an implantable device, as it may conform to various anatomical geometries for the treatment of different chronic diseases.

Acknowledgements

References

[1] F. Cui, C. He, L. Yin, F. Qian, M. He, C. Tang, C. Yin, Nanoparticles incorporated in bilaminated films: a smart drug delivery system for oral formulations, Biomacromolecules. 8 (9) (2007) 2845–2850.

[2] T.K. Jain, M.K. Reddy, M.A. Morales, D.L. Leslie-Pelecky, V. Labhasetwar, Biodistribution, clearance, and biocompatibility of iron oxide magnetic nanoparticles in rats, Molecular Pharmaceutics 5 (2) (2008) 316–327.

[3] F. Balas, M. Manzano, P. Horcajada, M. Vallet-Regi, Confinement and controlled release of bisphosphonates on ordered mesoporous silica-based materials, J. Am. Chem. Soc. 128 (25) (2006) 8116–8117.

[4] A. Peterson, T. Lopez, E. Ortiz Islas, R.D. Gonzalez, Pore structures in an implantable sol–gel ceramic device used in controlled drug release applications: a modeling study, Appl. Surf. Sci. 253 (2007) 5767–5771.

[5] Y. Zhang, D.W. Miller, Pathways for Drug Delivery to the Central Nervous System, Drug Delivery, Principles and Applications, John Wiley and Sons, Hoboken, 2005, pp. 29–56.

[6] T. Lopez, E. Ortiz Islas, P. Quintana, R.D. Gonzalez, A nanostructured titania bioceramic implantable device capable of drug delivery to the temporal lobe of the brain. Colloid and Surfaces A: Physicochem. Eng. Aspects 300 (2007) 3–10.

[7] T. Lopez, J. Navarette, R. Conde, J.A. Ascencio, J. Manjarrez, R.D. Gonzalez, A molecular vibrational analysis and MAS-NMR spectroscopy study of epilepsy drugs encapsulated in TiO₂–sol–gel reservoirs, J. Biomed. Mater. Res. A 78 (2006) 446–448.

[8] T. Lopez, E. Ortiz Islas, A. Hernandez, J. Manjarrez, F. Rodriguez-Reinoso, A. Sepulveda, R.D. Gonzalez, Biocompatible titania microtubes formed by nanoparticles and its application in the drug delivery of valproic acid, Opt. Mater. 29 (2006) 70–74.

[9] J.H. Prescott, S. Lipka, S. Baldwin, N.F. Sheppard Jr., J.M. Maloney, J. Coppeta, B. Yomtov, M.A. Staples, J.T. Santini Jr., Chronic, programmed polypeptide delivery from an implanted, multireservoir microchip device, Nat. Biotechnol. 24 (4) (2006) 437–438.

[10] A.K. Jain, R. Panchagnula, Skeletal drug delivery systems, Int J Pharm. 206 (2000) 1–12.

[11] S.H. Hu, T.Y. Liu, D.M. Liu, S.Y. Chen, Controlled pulsatile drug release from a ferrogel by a high-frequency magnetic field, Macromolecules 40 (19) (2007) 6786–6788.

[12] S.H. Hu, T.Y. Liu, H.Y. Huang, D.M. Liu, S.Y. Chen, Magnetic-sensitive silica nanospheres for controlled drug release, Langmuir. 24 (1) (2008) 239–244.

[13] J. Yang, J. Lee, J. Kang, C.H. Chung, K. Lee, J.S. Suh, H.G. Yoon, Y.M. Huh, S. Haam, Magnetic sensitivity enhanced novel fluorescent magnetic silica nanoparticles for biomedical applications, Nanotechnology 19 (2008) 1–6.

[14] S.K. Kurinec, N. Okeke, S.K. Gupta, H. Zhang, T.D. Xiao, Synthesis and electrophoretic deposition of magnetic nickel ferrite nanoparticles, J. Mater. Sci. 41 (2006) 8181–8185.

[15] T. Uchikoshia, T.S. Suzukia, H. Okuyamaa, Y. Sakkaa, P.S. Nicholsonb, Electrophoretic deposition of alumina suspension in a strong magnetic field, J. Eur. Ceram. Soc. 24 (2004) 225–229.

[16] F. Chicatun, J. Cho, S. Schaab, G. Brusatin, P. Colombo, J.A. Roether, A.R. Boccaccini, Lead zirconate titanate thick film prepared by electrophoretic deposition from oxide mixture, Advances in Applied Ceramics 106 (4) (2007) 186–195.

[17] H.G. Jeon, T. Sugiyama, H. Masuhara, T. Asahi, Study on electrophoretic deposition of size-controlled Quinacridone nanoparticles, J. Phys. Chem. C 111 (40) (2007) 14658–14663.

[18] F. Caruso, Colloids and Colloid Assemblies, vol. 14, Wiley-VCH, Weinheim, Germany, 2004, pp. 437–464.

[19] M. Trau, D.A. Saville, I.A. Akay, Assembly of colloidal crystals at electrode interfaceds, Langmuir. 13 (24) (1997) 6375–6381.

[20] M. Holgado, F. Garcı´a-Santamarı´a, A. Blanco, M. Ibisate, A. Cintas, H. Mı´guez, C. J. Serna, C. Molpeceres, J. Requena, A. Mifsud, F. Meseguer, C. Lo´pez, Electrophoretic deposition to control artificial opal growth, Langmuir. 15 (14) (1999) 4701–4704.

[21] S.H. Hu, T.Y. Liu, Y.H. Huang, D.M. Liu, S.Y. Chen, Stimuli-responsive controlled drug release from magnetic-sensitive silica nanospheres, J. Nanosci. Nanotechnol. 9 (2) (2009) 866–870.

[22] S. Santra, R.P. Bagwe, D. Dutta, J.T. Stanley, G.A. Walter, W. Tan, B.M. Moudgil, R.A. Mericle, Synthesis and characterization of fluorescent, radio-opaque, and paramagnetic silica nanoparticles for multimodal bioimaging applications, Adv. Mat. 17 (2005) 2165–2169.

[23] J.G. Sarver, K.A. Bachmann, D. Zhu, W.A. Klis, Ethosuximide is primarily metabolized by CYP3A when incubated with isolated rat liver microsomes, Dru. Mat. And Dep. 26 (1) (1998) 78–82.

[24] M. Stjerndahl, M. Andersson, H.E. Hall, D.M. Pajerowski, M.W. Meisel, R.S. Duran, Superparamagnetic Fe_3O_4/SiO_2 nanocomposites: enabling the tuning of both the iron oxide load and the size of the nanoparticles, Langmuir. 24 (7) (2008) 3532–3536.

[25] J.P. Manning, D.A. Richards, N. Leresche, V. Crunelli, N.G. Bowery, Cortical-area specific block of genetically determined absence seizures by ethosuximide, Neuroscience 123 (2004) 5–9.